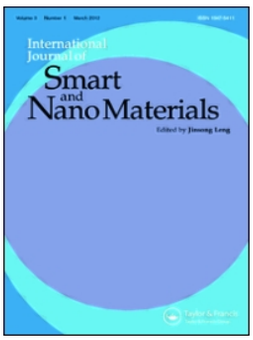

International Journal of Smart and Nano Materials

ISSN: (Print) (Online) Journal homepage: https://www.tandfonline.com/loi/tsnm20

Thickness and strain engineering of structural and electronic properties for 2D square-octagon AlN

Wantong Hou , Zhanbin Qi , Hang Zang , Yan Yan & Zhiming Shi

To cite this article: Wantong Hou , Zhanbin Qi , Hang Zang , Yan Yan & Zhiming Shi (2020) Thickness and strain engineering of structural and electronic properties for 2D square-octagon AlN, International Journal of Smart and Nano Materials, 11:3, 288-297, DOI: 10.1080/19475411.2020.1801879

To link to this article: https://doi.org/10.1080/19475411.2020.1801879

INTERNATIONAL JOURNAL OF SMART AND NANO MATERIALS
2020, VOL. 11, NO. 3, 288–297
https://doi.org/10.1080/19475411.2020.1801879

Taylor & Francis
Taylor & Francis Group

ARTICLE

OPEN ACCESS Check for updates

Thickness and strain engineering of structural and electronic properties for 2D square-octagon AlN

Wantong Hou[a,b], Zhanbin Qi[b], Hang Zang[b], Yan Yan[a] and Zhiming Shi[b]

[a]College of Science, Changchun University, Changchun, China; [b]State Key Laboratory of Luminescence and Applications, Changchun Institute of Optics, Fine Mechanics and Physics, Chinese Academy of Sciences, Changchun, China

ABSTRACT

Two-dimensional (2D) semiconductors exhibit great potential to minimize the size and drastically reduce the energy consumption of optoelectronic devices due to promising features induced by quantum confinement. It has achieved many successes in infrared and visible light optoelectronic devices. The study on ultra-wide band gap 2D semiconductors except *h*-BN are still limited, however, the requirement is more and more urgent. Inspired by the progresses of III-nitride semiconductors in recent several decades, 2D AlN is highly expected to be a new member of ultra-wide band gap 2D semiconductors. In this work, we employed the first-principles calculations to investigate the structural and electronic properties of 2D AlN. We revealed that few-layer AlN acquires a square-octagon (*so*-AlN) configuration in the vertical direction when the number of atomic layers *n* is smaller than 16. With increasing the thickness from 2 ML to 8 ML, the band gap decreased due to the weakening of quantum confinement effect. We demonstrated the intrinsic indirect band gap can be tuned to be direct by applying different direction strains for *so*-AlN. Our results open new avenues for their application in nano-optoelectronics.

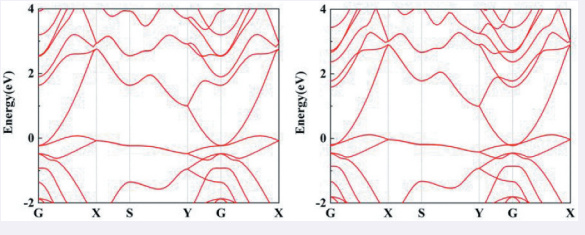

ARTICLE HISTORY
Received 18 May 2020
Accepted 23 July 2020

KEYWORDS
Square-octagon AlN; electronic structures; strain engineering; ultra-wide band gap semiconductors; first-principles calculation

Introduction

Inspired by the successful of graphene [1,2], a great deal of research efforts are devoted toward the investigation of two-dimensional (2D) materials in last decade [3,4]. The 2D

CONTACT Zhiming Shi shizm@ciomp.ac.cn State Key Laboratory of Luminescence and Applications, Changchun Institute of Optics, Fine Mechanics and Physics, Chinese Academy of Sciences, 3888 Dongnanhu Road, Changchun 130033, China

Supplemental data for this article can be accessed here.

materials not only exhibit unique and fascinating physical features by comparing their bulk counterpart [5–10], but also support a new dimension to tune the properties of by engineering the interlayer coupling [11–13]. The linear dispersion at *K* point endows novel phenomena in monolayer graphene, including the ultra-high mobility, fantastic thermal and electronic conduction and the anomalous room-temperature quantum Hall effect. The graphene-based devices have also been explored [5–7]. Transition from indirect to direct bandgap is revealed in transition-metal chalcogenides (TMCs) by reducing the thickness to monolayer [8–10]. Moreover, a large number of new 2D materials have been theoretically designed and experimentally realized, like monoelemental materials (silicene, germanene, phosphorene, borophene), MXenes, organic materials and nitrides. However, most existing 2D materials are metal or semiconductor, ultra-wide band gap 2D material is rarely achieved except hexagonal boron nitride (*h*-BN).

Aluminum nitride (AlN) is a promising ultra-wide band-gap material due to the good chemical stability, excellent thermal conductivity, high chemical resistance, and high melting point [14]. The devices based on AlN have already obtained significant success [15–18]. Therefore, 2D AlN is highly expected to be an essential supplement for ultra-wide band-gap 2D materials. Naturally, hexagonal AlN (*h*-AlN) nanosheet, similar to *h*-BN, is a promising material for optoelectronic applications. Following the good thermodynamic stability of *h*-AlN was theoretically confirmed [19], Tsipas et al. experimentally realized *h*-AlN via molecular beam epitaxy (MBE) [20]. Meanwhile, the studies on the electronic, optic, and magnetic properties of *h*-AlN are spread [21–23]. However, the MBE scheme is hard for economic applications due to the extreme high cost. Recently, 2D AlN within a few atomic layers has been realized by metalorganic chemical vapor deposition (MOCVD), which has already been widely used in semiconductor industry [24]. This exciting achievement greatly promotes the industrial applications of 2D AlN, in spite of the relevant research is still deficient.

Unlike *h*-BN, the ground state of AlN is in wurtzite configuration but not hexagonal configuration, therefore, the interlayer coupling is strong covalent bonds rather than vdW interaction. As a result, the monolayer *h*-AlN is quite unstable due to the large number of dangling bonds on the surface. Additionally, the *h*-AlN possesses an indirect band-gap [25,26], which limited the applications on lighting devices. Recently, the *h*-GaN was demonstrated to be unstable and reconstructed into a haeckelite phase with square-octagon (*so*-GaN) pattern and direct band-gap for few-layer thickness [27–29]. Naturally, the fundamental properties of 2D AlN is an interesting topic in ultra-wide band-gap semiconductors, however, the relevant research is still insufficient. Here, we employed the first-principles calculations based on density-functional theory (DFT) to investigate the structural and electronic properties for few-layer 2D AlN, which has obtained great success in 2D materials [30] and III-nitrides [31–33]. We found that the hexagonal structure (*h*-AlN) transferred into haeckelite (*so*-AlN) by adding the thickness higher than 4 ML, while the indirect band gap transferred to direct. The band gap decreased with increasing the thickness for *so*-AlN due to the quantum confinement effect. Moreover, we demonstrated that in-plane strain could effectively tune the electronic structures for few-layer *so*-AlN, which path a new way for their practical application in nano-electronics and nano-optoelectronics.

Methods

First-principles calculations were performed by employing the generalized gradient approximation (Perdew-Burke-Ernzerhof parametrization, PBE) and projector-augmented wave method, as implemented in the Vienna Ab-initio Simulation Package (VASP) [34]. The long-range noncovalent interactions was corrected by Grimme's dispersion (DFT-D3) [35,36]. A plane-wave basis set with the kinetic-energy of 500 eV was used. We employed $8 \times 4 \times 1$ Monkhorst-Pack k-grids in self-consistent calculations and 20 k-points between high symmetry points of the Brillouin zone in the band structure calculations. In addition, the force and total energy convergence thresholds were set to 0.01 eV/Å and 10^{-6} eV, respectively. The lattice parameter differences were smaller than 1% by comparing with experimental results of *w*-AlN. The simulation cells were built with vacuum slabs thicker than 20 Å to avoid artificial interaction of periodic images. The dangling bonds on the surfaces were passivated by hydrogen atoms and the thickness is defined by the number of layers (*n*ML, represent *n*-monolayers thick), as shown in Figure 1(a).

Results and discussions

Thickness-dependent geometry and electronic structures

The optimized structures of *so*-AlN and *w*-AlN are displayed in Figure 1(a). By comparing with the *w*-AlN, two differences can be observed. First, the *w*-AlN is still more stable than *so*-AlN by 78 meV per formula in bulk phase due to the *so*-AlN suffered considerable distortion. For *w*-AlN, the atoms keep ideal tetrahedral coordination with the bond angles are almost 109.5°. The case of *so*-AlN is a little different, one bond angle reduced to 90 ± 2° and others increased to 112.5 ± 1°. Second, the hexagon atomic arrangement transferred into square-octagon configuration along vertical direction.

In 2D AlN, the stability is terminated by two factors: (1) the bulk part and (2) the surface part. Undoubtedly, the bulk structure of *w*-AlN is more stable, however, the surface of *so*-AlN is energetically more favorable. The dynamical stability is confirmed by phonon calculation for 2 ML *so*-AlN as shown in Figure S1. According to Tasker's classification

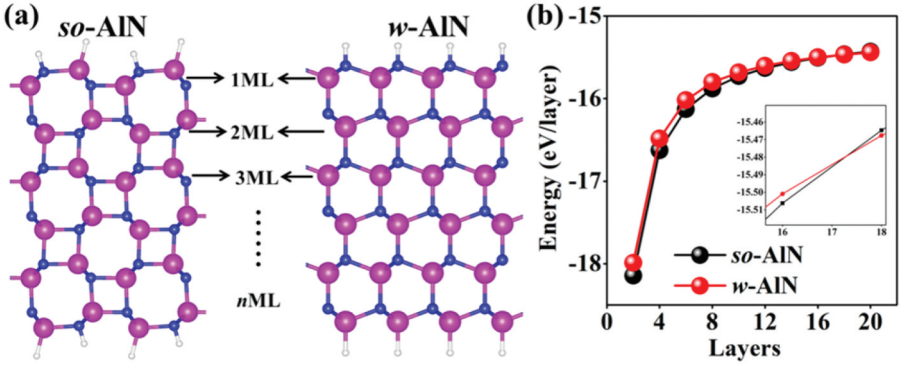

Figure 1. (a) The structures of 6 ML *so*-AlN (left) and *w*-AlN (right) are used as the examples of 2D AlN (N: blue, Ga: purple). (b) The energy per layer as the function of layers for *so*-AlN (black line) and *w*-AlN (red line). Inset is the zoom in of the crossing.

[37], the surface of *w*-AlN belongs to type-III, in which the cations or anions accumulated on opposite surfaces, respectively. The strong repulsion between the same charged on the surface resulted in intrinsically unstable due to the divergence of the surface energy. On the other hand, the surface of *so*-AlN is type-I surface with equal anions and cations on each plane, which should be more stable than type-III. This effect is subtle in bulk AlN, however, it played an important role in 2D AlN. The surface/bulk ratio of 2D AlN sharply increased with the reduction of material thickness. There should be a threshold that the high surface energy cannot be compensated by the bulk part, and the *w*-AlN will transform into *so*-AlN. We calculated the energy per layer and showed in Figure 1(b), the crossing appeared between 16 ML and 18 ML, indicating that the 2D *so*-AlN should be ground state for the structures thinner than 16 ML.

Next, we focused on the electronic structures of 2D *so*-AlN. First, the band structures for bulk *so*-AlN and *w*-AlN were calculated as the references, as shown in Figure 2(a,d). The direct band gap decreased from 4.18 eV for *w*-AlN to 3.85 eV for *so*-AlN. We plotted the spatial distribution of wavefunction for conduction band minimum (CBM) and valence band maximum (VBM) in insets of Figure 2(a,d). It is observed that the VBM was contributed by the N-p_z orbitals for *w*-AlN, but by N-p_x orbitals for *so*-AlN, while the CBMs were consistently contributed by N-*s* orbitals. Therefore, the raised energy level of VBM induced the band gap reduction of 2D *so*-AlN. With increasing the layer from 2 ML to 8 ML, the 2D *so*-AlN and *w*-AlN exhibited entirely different behavior. As shown in Figure 3, the band gap of 2 ML *w*-AlN was smaller than that of bulk phase and transformed to metal for the structures thicker than 4 ML, which was not consistent

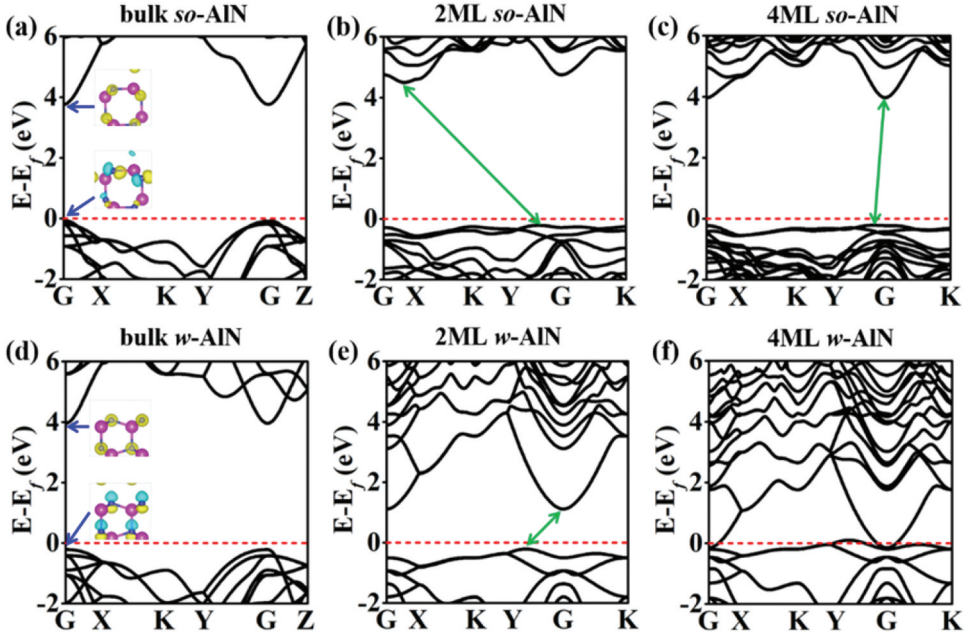

Figure 2. The band structures of (a, d) bulk, (b, e) 2 ML and (c, f) 4 ML *so*-AlN and *w*-AlN, the Fermi-level are set to zero and marked by red-dashed lines. The insets in (a) and (d) are the spatial distribution of wavefunction for VBM and CBM.

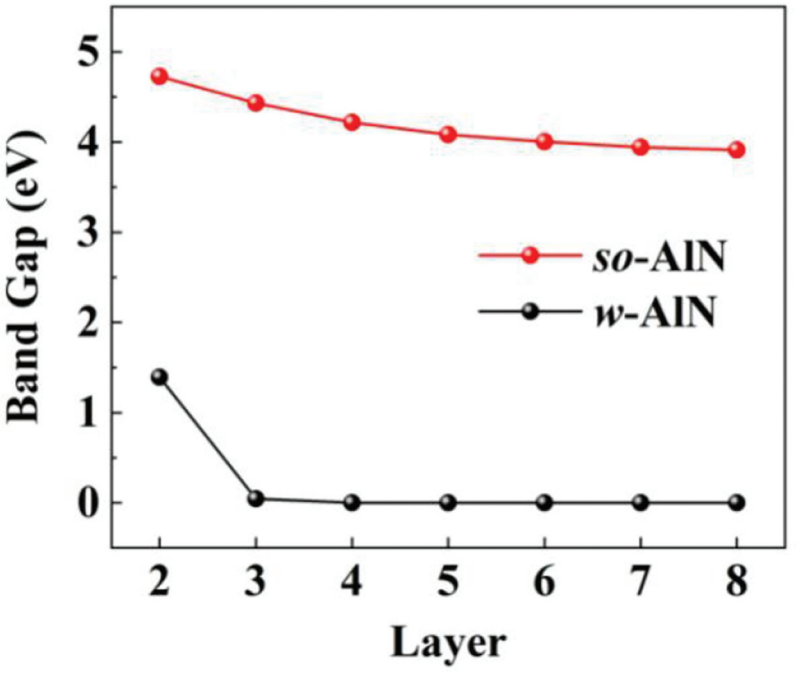

Figure 3. The band gaps as the function of *n*ML (n = 2–8) for 2D *so*-AlN and *w*-AlN.

with the normal quantum confinement effect. The similar mechanism has been reported in 2D gallium nitride [38], zinc dioxide [39], and boron nitride [40]. The evolution of the band edge states is shown in Figure S3. The absence of the N-*s* state during increasing the thickness may lower the energy level of CBM which leads metallization for 2D *w*-AlN. For 2D *so*-AlN, the band gap became larger due to the quantum confinement effect, and gradually closed to the band gap in bulk phase. Therefore, we can control the band gap from 4.76 to 3.85 eV by tuning the thickness for 2D *so*-AlN. The gapless for 2D w-AlN, limits the applications in optoelectronic devices, is overcame in 2D *so*-AlN. Moreover, the direct band gap changed into indirect band gap for both 2D *so*- and *w*-AlN. For 2 ML *w*-AlN (Figure 2(e)), the CBM is still at G point, and the VBM located between G→Y path. However, for 2 ML *so*-AlN (Figure 2(b)), the CBM located between G→X path, and the VBM located between G→Y path. After further increase the thickness, the CBM will still located at G point for 2D *so*-AlN. We also checked the effect of hydrogen-passivated on the band structures of 2D *so*-AlN, although it is practically unstable. The band gap variation with thickness for non-passivation 2D *so*-AlN is displayed in Figure S2. The dangling bonds on the surface induce a band gap reduction in thin slabs. The effect is decayed by increasing thickness, as a result, the band gap gradually increased.

Strain engineering of the electronic structures

The indirect band gap seriously hindered the applications of 2D *so*-AlN on lighting devices. It should be promising to realize direct band gap. The application of strain engineering in

2D materials is different from that in traditional materials, as nanomaterials are mechanically much stronger. We can apply far greater tensile stresses to tune their properties than is possible with traditional materials. Many reports have demonstrated that strain engineering is an effective tool to control the properties of 2D materials [41–43]. Here, we employed a 5 ML 2D *so*-AlN as an example and applied in-plane stress from −5% (compression) to 5% (tension) along the X, Y, and XY axes.

As shown in Figure 4(a-c), under uniaxial and biaxial strains, the effect on the length of shorter interatomic Al-N bonds was small, while the change for the longer interplane Al-N bonds was more significant. The influence of biaxial strain on distance was greater than that of uniaxial strain. First, we calculated the band structures under in-plane strain. The band gap variation with strain is displayed in Figure 4(d-f). Generally, the tensile stress resulted in band gap reduction for all directions strain. The effect of compression was a little different. The band gap monotonic increased with rising the uniaxial X and biaxial XY compression, however, the band gap first rose (0~-3%) and then dropped (<-3%) by strengthening uniaxial Y compression. We can observe that the indirect-direct band gap transition (yellow shadowed area in Figure 4(d-f)) can be realized by applying strain. Under uniaxial X strain, the transition occurred when the tensile stress was larger than 2%; under uniaxial Y strain, the transition occurred when the compression was larger than −1%; under biaxial XY, the transition occurred when the tensile stress was larger than 1% and the compression was larger than −2%. Therefore, the 2D *so*-AlN exhibited strong anisotropy response to strain.

To reveal the physical mechanism of strain engineering, we plotted the N-*p* orbital-projected band structures in Figures 5 and 6. We found the CBM always located at G point, therefore the indirect to direct band gap transition was governed by the change of VBM (marked by colored circles). Here, we neglected the conduction bands and just discussed

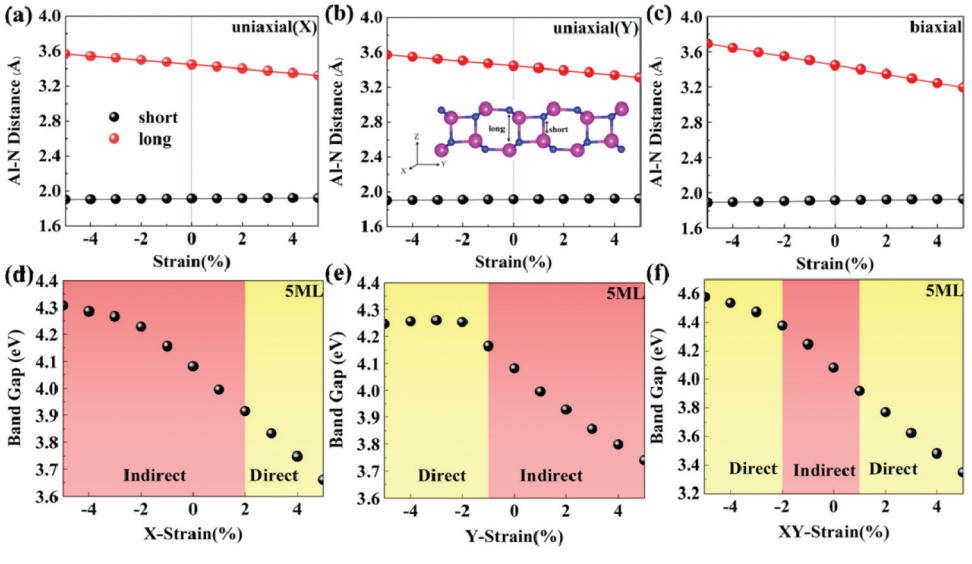

Figure 4. (a-c) Variations of the Al-N interatomic/interplane distances and (d-f) band gaps for 5 ML AlN slab under biaxial (left) and uniaxial strain applied along the X, Y and XY axes, respectively. Note that positive strain values correspond to tensile strain.

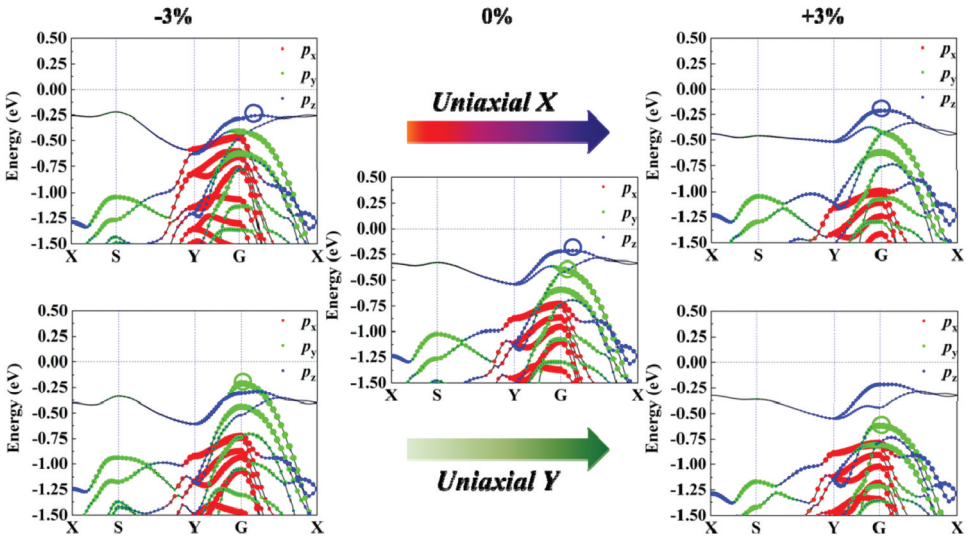

Figure 5. The N-*p* orbital-projected band structures for 5 ML *so*-AlN under uniaxial X (upper) and Y (down) strain. The red, green and blue dots represent p_x, p_y and p_z component. The Fermi-level are set to zero. The evolution of the VBM is marked by colored circles.

the effect of strain on valence bands near the Fermi-level. In strain-free structure, the VBM located at the point between G → X path and contributed by the p_z orbital. By applying strain along X axis, the VBM shifted to the G point under 3% tensile stress and the indirect band gap changed to be direct, due to the Al-N interplane distance was shortened, as discussed in Figure 4(a). The evolution of the VBM was marked by blue circles in Figure 5. It was observed that the VBM shifted close to the G point along the G → X path. On the other hand, the p_x states shifted up under compressive stress (−3%) due to the bond along X axis was shortened, however, the energy level was still lower than the p_z states. Under tensile stress (3%), the p_x states shifted down and away from the VBM. By applying strain along Y axis, the p_y states shifted up and became VBM at G point under −3% compressive stress and shifted down under 3% tensile stress. Therefore, the tensile stress along the X axis and compressive stress along the Y axis can induce the indirect to direct band gap transition. By applying biaxial strain, the effect was the superposition of uniaxial X and Y strain, as shown in Figure 6. The direct band gap was terminated by p_y states when the compressive stress was bigger than −2%, and by p_z when the tensile stress was bigger than 1%.

Conclusion

In summary, we systematically investigated the structural and band properties of 2D AlN by using first-principles calculations based on DFT. We found that the *so*-AlN structure was energetic more favorable than traditional *w*-AlN due to the unstable surface. According to our calculation, the *so*-AlN was the ground state when the number of atomic layer *n* was smaller than 16. The 2D *so*-AlN was an indirect band gap semiconductor, however, its bulk structures were direct band gap. With increasing the thickness from

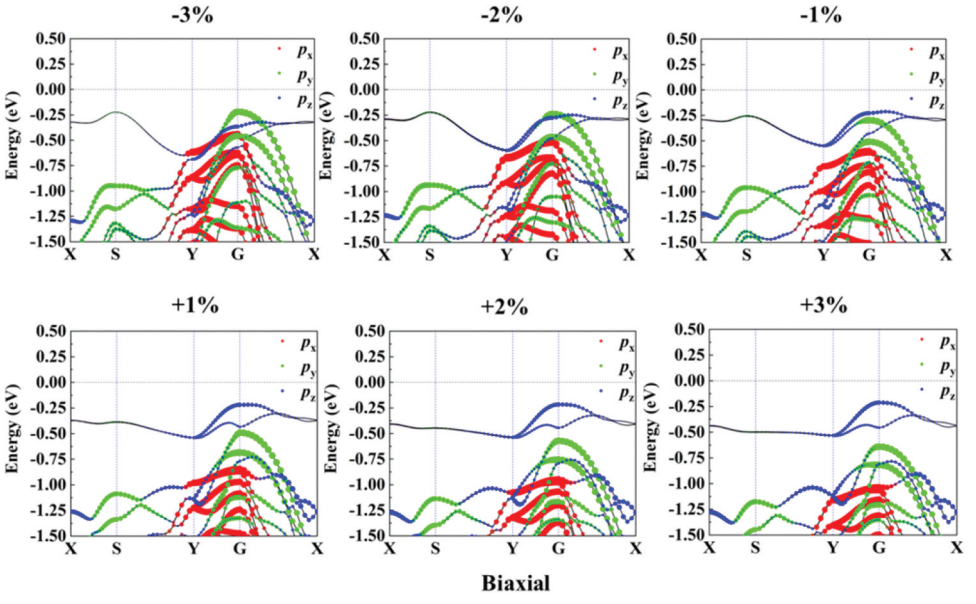

Figure 6. The N-*p* orbital-projected band structures for 5 ML *so*-AlN under biaxial strain. The red, green and blue dots represent p_x, p_y and p_z components. The Fermi-level are set to zero.

2 ML to 8 ML, the band gap decreased due to the weakening of quantum confinement effect. This entirely different from the case for 2D *w*-AlN. The intrinsic metallic behavior induced by the nearly free electron states and charge transfer between two surfaces has been overcome in 2D *so*-AlN. The indirect band gap can be tuned to be direct by applying in-plane strain. The 2D *so*-AlN exhibited strong anisotropy response to strain. We believe our results will significantly promote the applications of optoelectronic devices based on ultra-wide band gap semiconductors.

Acknowledgments

The research reported in this publication was supported by the National Natural Science Foundation of China (61804152 and 61834008), Key Research Program of Frontier Sciences, CAS (Grant No. ZDBS-LY-JSC026). It was also supported from the CAS Pioneer Hundred Talents Program.

Disclosure statement

No potential conflict of interest was reported by the authors.

Funding

This work was supported by the National Natural Science Foundation of China [61804152, 61834008].

ORCID

Zhiming Shi http://orcid.org/0000-0002-1207-570X

References

[1] Novoselov KS, Geim AK, Morozov S, et al. Two-dimensional gas of massless Dirac fermions in graphene. Nature. 2005;438:197.
[2] Novoselov KS, Geim AK, Morozov SV, et al. Electric field effect in atomically thin carbon films. Science. 2004;306:666.
[3] Bhimanapati GR, Lin Z, Meunier V, et al. Recent advances in two-dimensional materials beyond graphene. ACS Nano. 2015;9:11509.
[4] Butler SZ, Hollen SM, Cao L, et al. Progress, challenges, and opportunities in two-dimensional materials beyond graphene. ACS Nano. 2013;7:2898.
[5] Stankovich S, Dikin DA, Dommett GH, et al. Graphene-based composite materials. Nature. 2006;442:282.
[6] Kim KS, Zhao Y, Jang H, et al. Large-scale pattern growth of graphene films for stretchable transparent electrodes. Nature. 2009;457:706.
[7] Yang H, Heo J, Park S, et al. Graphene barristor, a triode device with a gate-controlled Schottky barrier. Science. 2012;336:1140.
[8] Zhang Y, Chang T-R, Zhou B, et al. Direct observation of the transition from indirect to direct bandgap in atomically thin epitaxial $MoSe_2$. Nat Nanotechnol. 2014;9:111.
[9] Ellis JK, Lucero MJ, Scuseria GE. The indirect to direct band gap transition in multilayered MoS_2 as predicted by screened hybrid density functional theory. Appl Phys Lett. 2011;99:261908.
[10] Luo N, Duan W, Yakobson BI, et al. Excitons and electron-hole liquid state in 2D γ-Phase Group-IV monochalcogenides. Adv Funct Mater. 2020;30:2000533.
[11] Chang T, Zhang H, Guo Z, et al. Nanoscale directional motion towards regions of stiffness. Phys Rev Lett. 2015;114:015504.
[12] Zhao J, Jiang J-W, Jia Y, et al. A theoretical analysis of cohesive energy between carbon nanotubes, graphene and substrates. Carbon. 2013;57:108.
[13] Liu Y, Weiss NO, Duan X, et al. Van der Waals heterostructures and devices. Nat Rev Mater. 2016;1:1.
[14] Strite S, Morkoç H. GaN, AlN, and InN: a review. J Vac Sci Technol B. 1992;10:1237.
[15] Davis RF. III-V nitrides for electronic and optoelectronic applications. Proc IEEE. 1991;79:702.
[16] Zhao S, Connie A, Dastjerdi M, et al. Aluminum nitride nanowire light emitting diodes: breaking the fundamental bottleneck of deep ultraviolet light sources. Sci Rep. 2015;5:8332.
[17] Taniyasu Y, Kasu M. Aluminum nitride deep-ultraviolet light-emitting p–n junction diodes. Diamond Relat Mater. 2008;17:1273.
[18] Liu D, Cho SJ, Park J, et al. 229 nm UV LEDs on aluminum nitride single crystal substrates using p-type silicon for increased hole injection. Appl Phys Lett. 2018;112:081101.
[19] Şahin H, Cahangirov S, Topsakal M, et al. Monolayer honeycomb structures of group-IV elements and III-V binary compounds: first-principles calculations. Phys Rev B. 2009;80:155453.
[20] Tsipas P, Kassavetis S, Tsoutsou D, et al. Evidence for graphite-like hexagonal AlN nanosheets epitaxially grown on single crystal Ag (111). Appl Phys Lett. 2013;103:251605.
[21] Keçik D, Bacaksiz C, Senger RT, et al. Layer-and strain-dependent optoelectronic properties of hexagonal AlN. Phys Rev B. 2015;92:165408.
[22] Bacaksiz C, Sahin H, Ozaydin H, et al. Hexagonal AlN: dimensional-crossover-driven band-gap transition. Phys Rev B. 2015;91:085430.
[23] Shi C, Qin H, Zhang Y, et al. Magnetic properties of transition metal doped AlN nanosheet: first-principle studies. J Appl Phys. 2014;115:053907.

[24] Wang W, Zheng Y, Li X, et al. 2D AlN layers sandwiched between graphene and Si substrates. Adv Mater. 2019;31:1803448.
[25] Bacaksiz C, Sahin H, Ozaydin H, et al. Hexagonal AlN: dimensional-crossover-driven band-gap transition. Phys Rev B. 2015;91:085430.
[26] de Almeida E, de Brito Mota F, de Castilho C, et al. Defects in hexagonal-AlN sheets by first-principles calculations. Eur Phys J B. 2012;85:48.
[27] Camacho-Mojica DC, López-Urías F. GaN haeckelite single-layered nanostructures: monolayer and nanotubes. Sci Rep. 2015;5:17902.
[28] Kolobov A, Fons P, Tominaga J, et al. Instability and spontaneous reconstruction of few-monolayer thick GaN graphitic structures. Nano Lett. 2016;16:4849.
[29] Kolobov A, Fons P, Saito Y, et al. Strain engineering of atomic and electronic structures of few-monolayer-thick GaN. Phys Rev Mater. 2017;1:024003.
[30] Xu R, Zou X, Liu B, et al. Computational design and property predictions for two-dimensional nanostructures. Mater Today. 2018;21:391.
[31] Vogel D, Krüger P, Pollmann J. Structural and electronic properties of group-III nitrides. Phys Rev B. 1997;55:12836.
[32] Van de Walle CG, Neugebauer J. First-principles calculations for defects and impurities: applications to III-nitrides. J Appl Phys. 2004;95:3851.
[33] Shi Z, Sun X, Jia Y, et al. Construction of van der Waals substrates for largely mismatched heteroepitaxy systems using first principles. Sci China Phys Mech. 2019;62:127311.
[34] Kresse G, Joubert D. From ultrasoft pseudopotentials to the projector augmented-wave method. Phys Rev B. 1999;59:1758.
[35] Grimme S. Semiempirical GGA-type density functional constructed with a long-range dispersion correction. J Comput Chem. 2006;27:1787.
[36] Barone V, Casarin M, Forrer D, et al. Role and effective treatment of dispersive forces in materials: polyethylene and graphite crystals as test cases. J Comput Chem. 2009;30:934.
[37] Tasker P. The stability of ionic crystal surfaces. J Phys C: Solid State Phys. 1979;12:4977.
[38] Freeman CL, Claeyssens F, Allan NL, et al. Graphitic nanofilms as precursors to wurtzite films: theory. Phys Rev Lett. 2006;96:066102.
[39] Wander A, Schedin F, Steadman P, et al. Stability of polar oxide surfaces. Phys Rev Lett. 2001;86:3811.
[40] Zhang Z, Guo W. Intrinsic metallic and semiconducting cubic boron nitride nanofilms. Nano Lett. 2012;12:3650.
[41] Zhu Z, Cheng Y, Schwingenschlögl U. Band inversion mechanism in topological insulators: A guideline for materials design. Phys Rev B. 2012;85:235401.
[42] Liu W, Peng X, Tang C, et al. Anisotropic interactions and strain-induced topological phase transition in Sb_2Se_3 and Bi_2Se_3. Phys Rev B. 2011;84:245105.
[43] Bertolazzi S, Brivio J, Kis A. Stretching and breaking of ultrathin MoS_2. ACS Nano. 2011;5:9703.